Effects of Hydrophilic Chain Length on the Characteristics of the Micelles of Pentaoxyethylene *n*-Decyl $C_{10}E_5$ and Hexaoxyethylene *n*-Decyl $C_{10}E_6$ Ethers

Kiyoe Imanishi and Yoshiyuki Einaga*

Department of Chemistry, Nara Women's University, Nara 630-8506, Japan

Received: December 19, 2004; In Final Form: February 15, 2005

Wormlike micelles of nonionic surfactants pentaoxyethylene decyl ether $C_{10}E_5$ and hexaoxyethylene decyl ether $C_{10}E_6$ in dilute aqueous solutions were characterized by static (SLS) and dynamic light scattering (DLS) experiments at several temperatures T below the critical points. The SLS results were analyzed with the aid of the molecular thermodynamic theory for SLS from micelle solutions formulated with the wormlike spherocylinder model, thereby yielding the molar mass M_w of the micelles as a function of c and the cross-sectional diameter d of 2.6 nm for both $C_{10}E_5$ and $C_{10}E_6$ micelles. It has been found that the micelles grow in size with increasing c and T, following the relation $M_w \propto c^{1/2}$ in conformity with the theoretical prediction for highly extended polymerlike micelles. The hydrodynamic radius R_H of the micelles as a function of M_w was found to be also well described by the corresponding theories for the wormlike spherocylinder model. The results of the stiffness parameter λ^{-1} show that both micelles are rather stiff compared with those formed with other polyoxyethylene alkyl ethers C_iE_j but far from rigid rods. The values of the spacing s between two adjacent hexaoxyethylene chains on the micellar surface were found to be substantially the same for both micelles.

Introduction

In recent work on dilute solutions of wormlike micelles of polyoxyethylene alkyl ethers $CH_3(CH_2)_{i-1}(OCH_2CH_2)_jOH$, abbreviated C_iE_j, we have investigated weight-average molar mass M_w of micelles as a function of surfactant mass concentration c and temperature T, along with the hydrodynamic radius R_H and mean-square radius of gyration $\langle S^2 \rangle$ by static (SLS) and dynamic light scattering (DLS).[1,2] The wormlike micelles studied were formed in the L_1 phase below the lower consolute phase boundary with hexaoxyethylene dodecyl $C_{12}E_6$ and tetradecyl $C_{14}E_6$ ethers,[1] and octaoxyethylene tetradecyl $C_{14}E_8$, hexadecyl $C_{16}E_8$, and octadecyl $C_{18}E_8$ ethers.[2] To evaluate separately two concentration-dependent contributions of micellar growth and intermicellar interactions to SLS results, the SLS data were analyzed by using a molecular thermodynamic theory of light scattering for micelle solutions formulated with the wormlike spherocylinder model,[3] thereby yielding the M_w values of the micelles present at a specific c.

It has been found that M_w increases as $M_w \propto c^{1/2}$ in agreement with the theoretical prediction derived on the basis of the association−dissociation equilibria for wormlike micelles.[3−5] In addition, the dependence of both R_H and $\langle S^2 \rangle$ on M_w has been quantitatively represented by the theories based on the wormlike spherocylinder and chain models, respectively.[6−9] From these comparisons of experimental observations with theoretical results, we have determined the values of the cross-sectional diameter d, contour length L, and stiffness parameter λ^{-1} of the wormlike spherocylindrical micelles. To visualize micellar structure, the spacing s between adjacent hydrophilic groups, that is, oxyethylene groups, of the C_iE_j molecules on the micellar surface has been calculated from these parameters along with the partial specific volume υ of the micelles.

In agreement with literature results,[10] the cloud point temperature (LCST) of the micelle solutions of the surfactant molecules C_iE_j significantly decreased with increasing alkyl chain length i when the oxyethylene chain length j was fixed to 6 or 8. Accompanying these phase variations, the micellar length has been appreciably longer for larger i when compared at fixed c and T. On the contrary, neither the cross-sectional diameter d nor spacing s vary with i to a great extent. These findings indicate that the micelle structures, that is, arrangements of the C_iE_j molecules in the micelles, are the same in a quantitative sense without regard to the hydrophobic chain length.

In the present work, we have characterized polymerlike micelles formed with pentaoxyethylene decyl $C_{10}E_5$ and hexaoxyethylene decyl $C_{10}E_6$ ethers in dilute aqueous solution by SLS and DLS measurements. The aim is to examine the effects of the hydrophilic chain length, or oxyethylene chain length, on the structure and size of the micelles. To this end, we have determined the values of d, L, λ^{-1}, and s of the micelles by applying the same technique as employed in the previous studies.[1,2]

Experimental Section

Materials. High-purity $C_{10}E_5$ and $C_{10}E_6$ samples were purchased from Nikko Chemicals Co. Ltd. and used without further purification. The nominal value of purity is higher than 99% for both samples. The solvent water was high purity (ultrapure) water prepared with a Simpli Lab water purification system of Millipore Co.

Phase Diagram. The cloud-point temperature of a solution was determined as the temperature at which the intensity of the (laser) light transmitted through the solution abruptly decreased with increasing temperature.

Static Light Scattering. SLS measurements were performed at temperatures T ranging from 25.0 to 42.0 °C for $C_{10}E_5$ micelle solutions and from 30.0 to 60.0 °C for $C_{10}E_6$ micelle solutions.

10.1021/jp044226q CCC: $30.25
Published on Web 03/16/2005

The apparatus used is an ALV DLS/SLS-5000/E light-scattering photogoniometer and correlator system with vertically polarized incident light of 632.8 nm wavelength from a Uniphase Model 1145P He-Ne gas laser. For a calibration of the apparatus, the intensity of light scattered from pure benzene was measured at 25.0 °C at a scattering angle of 90° without an analyzer before the detector, taking the Rayleigh ratio $R_{Uv}(90)$ of pure benzene for unpolarized scattered light with polarized incident light at a wavelength of 632.8 nm to be 11.84×10^{-6} cm^{-1}.[11,12]

The $C_{10}E_5$ and $C_{10}E_6$ micelle solutions were prepared by dissolving the appropriate amount of the surfactant samples in water. Complete mixing and micelle formation were achieved by stirring the mixture for at least 1 day with a magnetic stirrer. The solutions thus prepared were optically purified by filtration through a membrane of 0.20 μm pore size at ambient temperature ca. 22 °C. The weight concentrations w of the solutions were determined gravimetrically and converted to mass concentrations c by the use of the densities ρ of the solutions given below.

The scattering intensities were measured for each solution and for the solvent water at scattering angles θ ranging from 30° to 150°. Data points of $Kc/\Delta R_\theta$ at fixed c plotted against $\sin^2(\theta/2)$ followed a straight line whose slope was negligibly small. From the extrapolation of the data to zero scattering angle for a given solution, we evaluated $Kc/\Delta R_0$, where ΔR_0 is the excess Rayleigh ratio, and K is the optical constant defined as

$$K = \frac{4\pi^2 n^2 (\partial n/\partial c)_{T,p}^{\ 2}}{N_A \lambda_0^{\ 4}} \quad (1)$$

with n being the refractive index of the solution, N_A the Avogadro's number, λ_0 the wavelength of the incident light in a vacuum, and $(\partial n/\partial c)_{T,p}$ the refractive index increment.

The values of $(\partial n/\partial c)_{T,p}$ at 632.8 nm were measured at 20.0, 30.0, and 40.0 °C for the $C_{10}E_5$ micelle solutions and at 30.0, 40.0, and 50.0 °C for the $C_{10}E_6$ micelle solutions, using a Union Giken R601 differential refractometer. The results were represented as $(\partial n/\partial c)_{T,p} = 0.1317 - (2.075 \times 10^{-4})(T - 273.15)$ cm^3/g for the former and $(\partial n/\partial c)_{T,p} = 0.1290 - (1.720 \times 10^{-4})$-$(T - 273.15)$ cm^3/g for the latter.

Dynamic Light Scattering. DLS measurements were carried out for the same micelle solutions at the same temperatures with the apparatus and light source described above for the SLS studies. The normalized autocorrelation function $g^{(2)}(t)$ of the scattered light intensity $I(t)$, i.e.,

$$g^{(2)}(t) = \langle I(0)I(t)\rangle/\langle I(0)\rangle^2 \quad (2)$$

was measured at scattering angles θ ranging from 30° to 150°. To acquire the statistical accuracy, measurements were performed for sufficiently long time so that more than 10^8 counts of photons were accumulated. From the data for $g^{(2)}(t)$, we determined D by the equations

$$(1/2)\ln[g^{(2)}(t) - 1] = (1/2)\ln f - K_1 t + \ldots \quad (3)$$

$$D = \lim_{q\to 0} K_1/q^2 \quad (4)$$

Here, f is the coherence factor, fixed by the optical system, K_1 is the first cumulant, and q is the magnitude of the scattering vector, defined as

$$q = \frac{4\pi n}{\lambda_0}\sin(\theta/2) \quad (5)$$

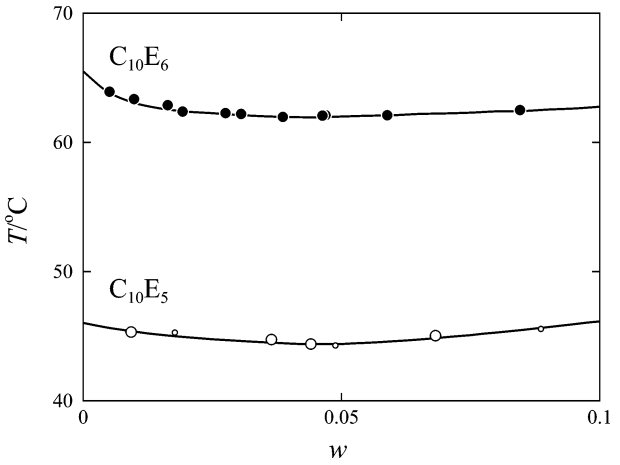

Figure 1. Phase diagrams of the $C_{10}E_5$ + water (unfilled circles) and the $C_{10}E_6$ + water (filled circles) systems: large circles, present cloud point data; small unfilled circles, cloud point data by Lang and Morgan.[13]

It is to be noted that the D values should be regarded as an average, since the micelles observed may have distribution in size.

In this work, we have not taken into account the effects of multiple scattering and intermicellar entanglement interactions that may possibly appear at high temperature and concentration, since the indication of such effects has not been found in the present observations.

Density. The density ρ required to calculate c and v was measured at 20.0, 30.0, and 40.0 °C for $C_{10}E_5$ micelle solutions, and 30.0, 40.0, and 50.0 °C for $C_{10}E_6$ micelle solutions, using a pycnometer of the Lipkin-Devison type. The results are summarized as (in cm^3/g)

$$\rho^{-1} = 0.9956 + (3.03 \times 10^{-4})(T - 273.15) + (4.46 \times 10^{-2})w \quad (6)$$

$$v = 1.042 + (3.03 \times 10^{-4})(T - 273.15) \quad (7)$$

for $C_{10}E_5$ micelle solutions and

$$\rho^{-1} = 0.9929 + (4.08 \times 10^{-4})(T - 273.15) \quad (8)$$

$$v = 0.9929 + (4.08 \times 10^{-4})(T - 273.15) \quad (9)$$

for $C_{10}E_6$ micelle solutions.

Results

Phase Behavior. Figure 1 illustrates phase diagrams of the $C_{10}E_5$ + water (unfilled circless) and $C_{10}E_6$ + water (filled circles) systems, where the circles represent cloud points. The results obtained here for the former system are in good agreement with the literature data reported by Lang and Morgan,[13] shown as the small circles. The critical temperature T_c is 44.3 °C for the $C_{10}E_5$ system and 62.1 °C for the $C_{10}E_6$ system. The former is about 17.8 °C lower than the latter, in accord with literature data summarized by Huibers et al.[10] This phase behavior indicates that the length of the hydrophilic or the oxyethylene chain has significant effects on the properties of the micelle solutions.

Static Light Scattering. The results of $Kc/\Delta R_0$ are shown as a function of c for the $C_{10}E_5$ and $C_{10}E_6$ micelle solutions at several temperatures in Figures 2 and 3, respectively. The data points at fixed T follow a smooth curve convex downward

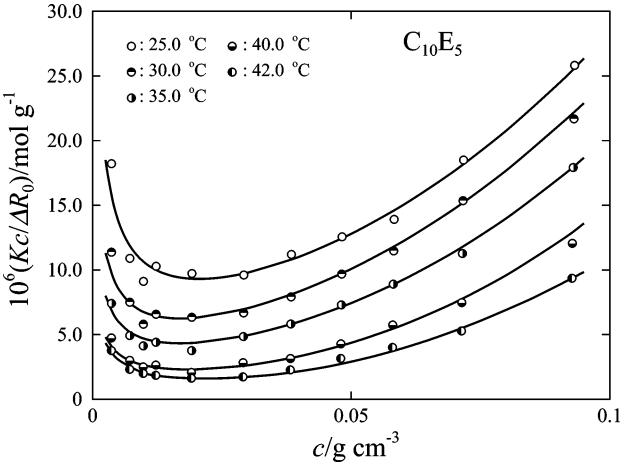

Figure 2. Plots of $Kc/\Delta R_0$ against c for the $C_{10}E_5$ solutions at various T: unfilled circles, 25.0 °C; top-half-filled circles, 30.0 °C; right-half-filled circles, 35.0 °C; bottom-half-filled circles, 40.0 °C; left-half-filled circles, 42.0 °C.

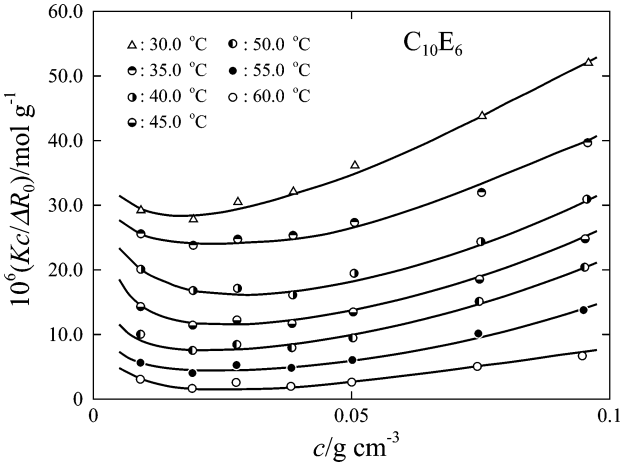

Figure 3. Plots of $Kc/\Delta R_0$ against c for the $C_{10}E_6$ solutions at various T: triangles, 30.0 °C; top-half-filled circles, 35.0 °C; right-half-filled circles, 40.0 °C; bottom-half-filled circles, 45.0 °C; left-half-filled circles, 50.0 °C; filled circles, 55.0 °C; unfilled circles, 60.0 °C.

whose curvature becomes less significant as T is increased. The $Kc/\Delta R_0$ value at fixed c decreases with increasing T.

Dynamic Light Scattering. The values of D for all the solutions examined are listed in Tables 1 and 2, and plotted against c in Figures 4 and 5 for the $C_{10}E_5$ and $C_{10}E_6$ micelle solutions, respectively, at various fixed temperatures. For each micelle solution, the data points at fixed T follow a curve concave upward as indicated, whereas at fixed c, D decreases with increasing T.

Discussion

Analysis of SLS Results. A classical result for the mean contour length $\langle L\rangle$ of polymeric micelles has been derived as

$$\langle L\rangle \simeq \phi^{1/2}\exp(E_{sc}/2k_BT) \tag{10}$$

using a mean-field approach, such as Flory−Huggins theory.[4,14] Here, ϕ is the surfactant volume fraction, k_B is the Boltzman constant, and E_{sc} is defined as the energy required to create two hemispherical end caps as the result of scission of a rodlike micelle. Recent treatments[3,5,15,16] of multiple equilibrium between micelles of different sizes and monomers give the number-average aggregation number N_n as

$$N_n \propto \phi^{1/2}\exp(\Delta g/k_BT) \tag{11}$$

for well-developed micellar systems. Here, Δg is the micellization free energy, comprising two factors: (1) the difference between the free energy density of threadlike micelle in the end-

TABLE 1: Values of M_w, D, $R_{H,app}$, and L_w for the $C_{10}E_5$ Micelles

c/g cm^{-3}	$10^{-4}M_w$	10^7D/cm^2 s^{-1}	$R_{H,app}$/nm	L_w/nm
		$T = 25.0$ °C		
0.003 6576	6.53			21.4
0.007 2120	9.11			29.6
0.0098368	10.6	3.83	6.08	34.4
0.012285	11.9	4.47	6.55	38.3
0.019208	14.9	4.30	7.95	47.8
0.029242	18.5	4.09	10.0	59.1
0.038444	21.3	4.06	13.3	68.1
0.048243	24.0	4.08	16.4	76.6
0.058307	26.6	4.12	19.5	84.7
0.071728	29.8	4.47	26.1	94.9
0.093204	34.6	4.81	37.4	110
		$T = 30.0$ °C		
0.0036525	10.6			34.4
0.0072019	14.9			47.8
0.0098232	17.4	3.65	7.56	55.8
0.012268	19.5	4.09	8.51	62.3
0.019182	24.4	3.85	10.8	77.9
0.029202	30.3	3.67	14.5	96.3
0.038390	34.9	3.71	19.2	111
0.048176	39.3	3.75	25.6	125
0.058226	43.5	3.86	31.9	138
0.071629	48.7	4.18	42.9	154
0.093075	56.3	4.68	59.7	178
		$T = 35.0$ °C		
0.0036467	15.0			48.2
0.0071905	21.1			67.2
0.0098076	24.6	3.32	9.40	78.4
0.012249	27.5	3.57	10.4	87.6
0.019151	34.5	3.29	11.9	110
0.029155	42.7	3.22	19.0	135
0.038330	48.9	3.23	25.5	155
0.048099	55.2	3.45	33.2	175
0.058134	60.9	3.50	43.0	193
0.071516	68.0	3.78	54.8	215
0.092928	78.2	4.27	84.7	247
		$T = 40.0$ °C		
0.0036402	24.6			78.5
0.0071777	34.6			110
0.0097902	40.4	2.88	12.0	128
0.012227	45.1	2.86	14.2	143
0.019117	56.5	2.55	15.3	178
0.029104	69.7	2.37	27.3	221
0.038262	80.0	2.41	33.6	253
0.048014	89.8	2.62	46.2	284
0.058031	98.8	2.73	64.0	312
0.071389	110	2.96	83.2	347
0.092764	126	3.47	125	397
		$T = 42.0$ °C		
0.0036374	31.6			100
0.0071722	44.4			141
0.0097827	51.8	2.43	15.3	164
0.012217	57.9	2.47	15.5	183
0.019103	72.3	2.10	19.8	229
0.029081	89.3	1.84	28.8	282
0.038232	102	1.93	40.7	323
0.047977	115	2.18	55.1	362
0.057987	126	2.20	74.5	398
0.071335	140	2.47	94.2	442
0.092693	160	3.00	150	505

TABLE 2: Values of M_w, D, $R_{H,app}$, and L_w for the $C_{10}E_6$ Micelles

c/g cm^{-3}	$10^{-4}M_w$	10^7D/cm^{2}s^{-1}	$R_{H,app}$/nm	L_w/nm
		$T = 30.0$ °C		
0.0092183	2.78			11.1
0.019374	3.98			15.5
0.027991	4.80			18.5
0.038731	5.70			21.9
0.050648	6.62			25.2
0.075280	8.35			31.6
0.095867	9.72			36.7
		$T = 35.0$ °C		
0.0092037	2.11			8.60
0.019343	2.88			11.4
0.027947	3.39			13.4
0.038669	3.95			15.4
0.050568	4.50			17.4
0.075161	5.51			21.2
0.095714	6.28			24.0
		$T = 40.0$ °C		
0.0091873	5.13	4.63	7.68	14.9
0.019308	7.36	5.92	7.06	21.0
0.027897	8.88	6.19	8.16	25.1
0.038600	10.5	6.54	8.42	29.6
0.050478	12.2	6.18	12.1	34.1
0.075027	15.2	6.70	16.6	42.4
0.095544	17.6	6.57	23.8	48.9
		$T = 45.0$ °C		
0.0091568	7.46	4.96	8.27	21.3
0.019244	10.8	5.90	7.87	30.4
0.027804	13.0	6.46	9.12	36.5
0.038472	15.4	6.24	10.4	43.1
0.050310	17.8	5.98	14.1	49.5
0.074778	22.2	6.09	22.6	61.5
0.095226	25.5	6.60	30.6	70.6
		$T = 50.0$ °C		
0.0091481	12.1	7.62	6.78	34.0
0.019226	17.6	5.69	9.70	49.0
0.027778	21.2	5.59	13.1	58.9
0.038436	25.1	5.03	15.9	69.6
0.050262	28.9	5.14	20.8	80.0
0.074707	35.8	5.90	34.0	98.9
0.095136	41.0	6.13	48.3	113
		$T = 55.0$ °C		
0.0091269	18.8	6.25	7.94	52.5
0.019182	27.3	4.44	11.4	75.7
0.027714	32.8	4.77	16.3	90.9
0.038347	38.7	3.42	24.1	107
0.050146	44.4	3.90	29.6	123
0.074534	54.5	4.57	49.3	150
0.094916	61.9	4.83	68.7	171
		$T = 60.0$ °C		
0.0091031	43.7	4.21	16.4	121
0.019131	63.3	3.24	16.0	175
0.027641	76.0	3.54	27.5	210
0.038246	89.4	2.71	31.4	247
0.050015	102	2.68	47.2	282
0.074339	125	2.73	103	344
0.094668	141	2.81	143	388

hemisphere portion and that in the middle-cylinder portion and (2) intermicellar interaction terms, that is, excluded volume contributions. In the limit of extensive micellar growth, it has been shown that the micellar size distribution becomes the most probable one, with N_w/N_n equal to 2, without regard to the presence of excluded-volume interactions.[5] It should be noted that N_w and N_n are related to the weight-average contour length L_w and the number-average L_n, respectively, as described below.

By formulating the intermicellar interactions with the wormlike spherocylinder model,[17] Sato[3] has derived the equation for light scattering of micelle solutions. The model consists of a

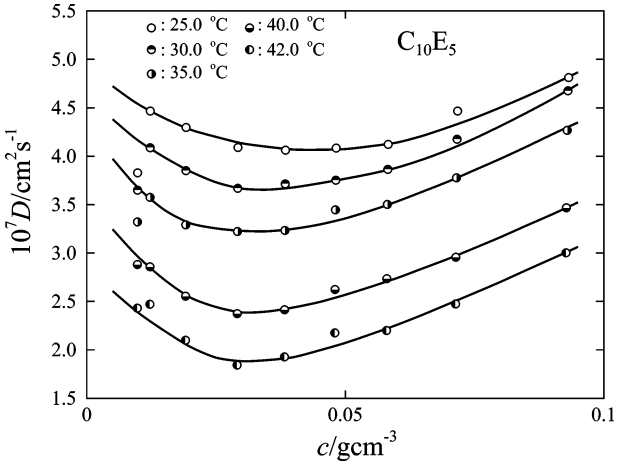

Figure 4. Plots of D against c for the $C_{10}E_5$ solutions at various T: the symbols have the same meaning as those in Figure 2.

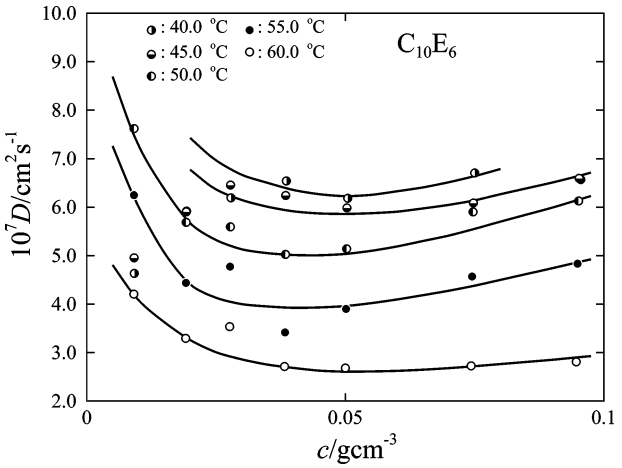

Figure 5. Plots of D against c for the $C_{10}E_6$ solutions at various T: the symbols have the same meaning as those in Figure 3.

wormlike cylinder of contour length $L - d$, cross-sectional diameter d, and two hemispheres of diameter d which cap the ends of the cylinder. As noted above, the stiffness of the wormlike cylinder is represented by the stiffness parameter λ^{-1}. When L is equal to d, the model becomes a sphere of diameter d. The result of $Kc/\Delta R_0$ may be put in the form

$$\frac{Kc}{\Delta R_0} = \frac{1}{M_w(c)} + 2A(c)c \qquad (12)$$

where $M_w(c)$ and $A(c)$ are the weight-average molar mass of the micelles and the apparent virial coefficient, respectively, obtained at concentration c. It should be noted that in principle $A(c)$ values include the second, third, and higher virial coefficient terms. The function $M_w(c)$ includes three parameters d, the strength $\hat{\epsilon}$ of the attractive interaction between spherocylinders (the depth of the attractive potential well given in terms of k_BT), and the free-energy parameter g_2, representing the difference in free energy of the surfactant molecules located in the end-capped portion from those in the middle-cylindrical portion in the micelle.

The apparent virial coefficient $A(c)$, which includes two parameters d and $\hat{\epsilon}$, has been formulated to describe thermodynamic properties of micelle solutions up to high concentrations by taking into account the hard-core repulsive interactions dominated by the parameter d, together with the attractive interactions dominated by the parameter $\hat{\epsilon}$ among the micelles.

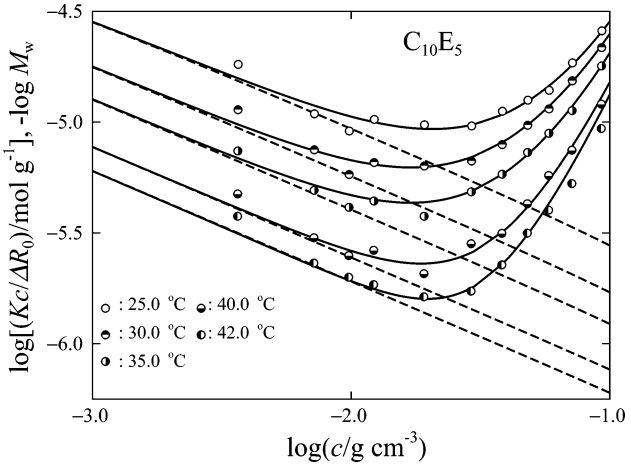

Figure 6. Double-logarithmic plots of $Kc/\Delta R_0$ against c for the $C_{10}E_5$ micelle solutions at various T: The symbols have the same meaning as those in Figure 2. The solid and dashed curves represent the calculated values of $Kc/\Delta R_0$ and $1/M_w(c)$, respectively.

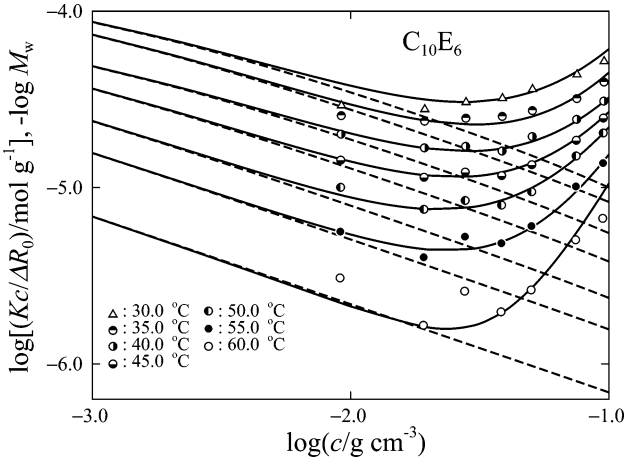

Figure 7. Double-logarithmic plots of $Kc/\Delta R_0$ against c for the $C_{10}E_6$ micelle solutions at various T: The symbols have the same meaning as those in Figure 3. The solid and dashed curves represent the calculated values of $Kc/\Delta R_0$ and $1/M_w(c)$, respectively.

Since the expressions for the functions $M_w(c)$ and $A(c)$ are rather complicated, the reader is referred to details in the original papers.[3,17] For convenience, we briefly describe the equations and procedure required to calculate $Kc/\Delta R_0$ in the Appendix.

The model may represent a variety of shapes of polymer-like micelles, including a sphere, rigid rod, and flexible and/or random-coil rod (or cylinder). In this work, we have analyzed the SLS results to determine the values of M_w of the $C_{10}E_5$ and $C_{10}E_6$ micelles at finite concentrations according to eq 12. In practice, we have determined the best-fit theoretical values of $Kc/\Delta R_0$ as a function of c to the experimental data at fixed T, as shown in Figures 2 and 3, by selecting d, g_2, and $\hat{\epsilon}$, thereby obtaining the $M_w(c)$ values at finite concentrations at each given T. The results are depicted in bilogarithmic plots in Figures 6 and 7 for the $C_{10}E_5$ and $C_{10}E_6$ micelle solutions, respectively. Here the solid and dashed curves represent the calculated values of $Kc/\Delta R_0$ and $1/M_w(c)$, respectively. It is seen that the solid curve for each solution at a given temperature coincides well with the corresponding data points, implying that the $C_{10}E_5$ and $C_{10}E_6$ micelles in dilute aqueous solutions may be represented by the wormlike spherocylinder model. The d value chosen is 2.6 nm for both $C_{10}E_5$ and $C_{10}E_6$ micelles at any T examined.

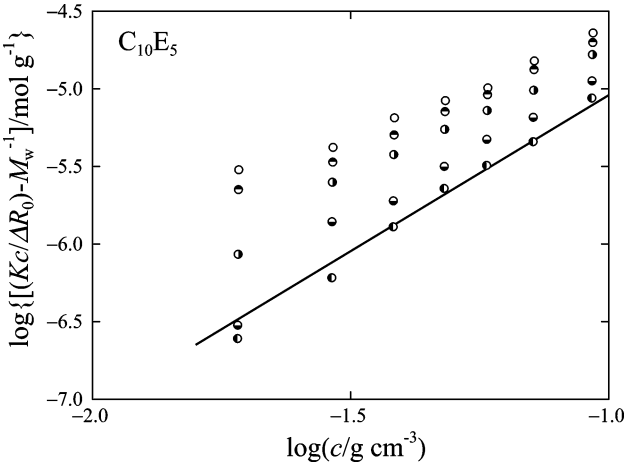

Figure 8. Double-logarithmic plots of $Kc/\Delta R_0 - M_w^{-1}$ against c for the $C_{10}E_5$ micelle solutions at various T: The symbols have the same meaning as those in Figure 2. The solid line has slope 2.

This value is almost comparable to, but slightly larger than, the values obtained previously[1,2] for other C_iE_j micelles.

In Figures 6 and 7, the dashed curve at any fixed T has a slope -0.5, showing that $M_w \propto c^{1/2}$ in the range of c studied, in accord with the simple theoretical results given by eq 11 or eq 10, since $\phi = \nu c$ and ν is nearly constant over the range of T and c studied. This behavior indicates that the $C_{10}E_5$ and $C_{10}E_6$ micelles are sufficiently extended to correspond to the theoretical predictions mentioned above. The M_w values at observed concentrations c are summarized in Tables 1 and 2 for the $C_{10}E_5$ and $C_{10}E_6$ micelles, respectively. The solid and dashed curves coincide with each other at small c, with the difference between them steadily increasing with increasing c. The results indicate that contributions of the virial coefficients to $Kc/\Delta R_0$, i.e., the second term of the right-hand side of eq 12, are negligible in comparison with the effects of increasing molar mass of the micelle at small c but progressively increase with increasing c as expected. It is seen in Figure 6 that the data points at different T tend to approach one another as c is increased, suggesting that the thermodynamic properties of the $C_{10}E_5$ micelle solutions may follow the relation $A(c)c \propto c^2$, independent of M_w, predicted for the range of moderately concentrated or semiconcentrate solutions of real polymers.[18,19] To confirm this point, $Kc/\Delta R_0 - M_w^{-1}$ is bilogarithmically plotted against c in Figure 8. The data at the highest T, i.e., 42.0 °C, follow a straight line with a slope of 2, in accord with the above relation, but those at the other T deviate upward from this line although they show a slight tendency to approach it. The results may imply that the $C_{10}E_5$ micelle solutions at c and T examined are still below the range of the moderately concentrated solutions.

The values of $\hat{\epsilon}$ and g_2 are plotted against T in Figures 9 and 10, respectively. It is found that when compared at fixed T, both parameters are larger for the $C_{10}E_5$ micelle solutions than with the $C_{10}E_6$ micelle solutions, and both are increasing functions of T.

Hydrodynamic Radius of the Micelle. The mutual diffusion coefficient D determined by eq 4 is in general described by[20,21]

$$D = \frac{(1 - \nu c)^2 M}{N_A \zeta} \left(\frac{\partial \pi}{\partial c}\right)_{T,p} \tag{13}$$

where M is the molar mass of the solute, ζ is the translational friction coefficient of the diffusing particle (micelle), and $(\partial\pi/\partial c)_{T,p}$ is the osmotic compressibility. Defining the hydro-

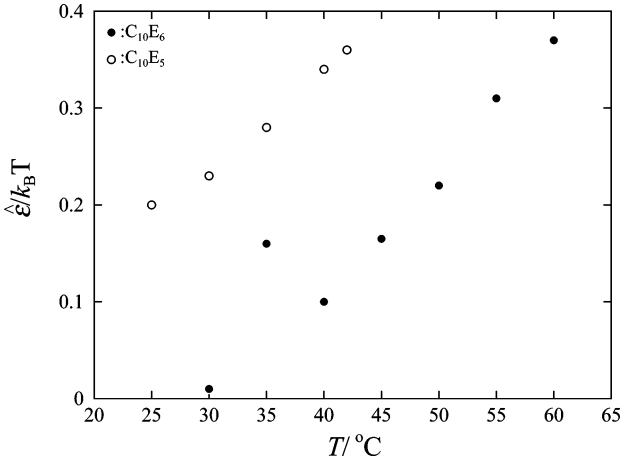

Figure 9. Temperature dependence of $\hat{\epsilon}/k_BT$ for the $C_{10}E_5$ + water (unfilled circles) and $C_{10}E_6$ + water (filled circles) systems.

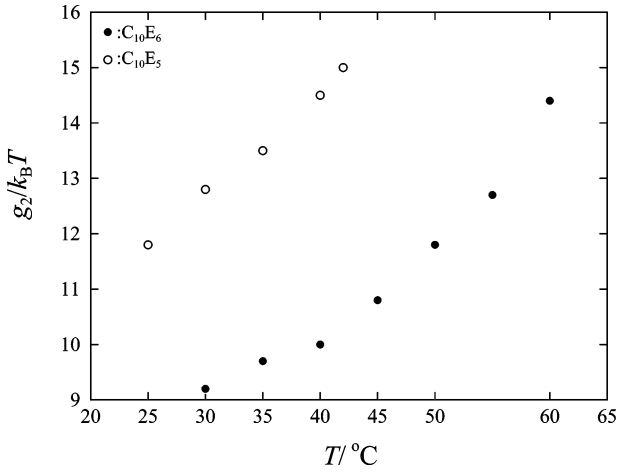

Figure 10. Temperature dependence of g_2/k_BT for the $C_{10}E_5$ + water (unfilled circles) and $C_{10}E_6$ + water (filled circles) systems.

dynamic radius $R_{H,app}$ (at finite concentrations) according to the Stokes law as

$$\zeta = 6\pi\eta_0 R_{H,app} \tag{14}$$

we obtain

$$D = \frac{(1 - \upsilon c)^2 M}{6\pi\eta_0 N_A R_{H,app}} \left(\frac{\partial\pi}{\partial c}\right)_{T,p} \tag{15}$$

from eq 13, where η_0 is the solvent viscosity.

We have evaluated $R_{H,app}$ by eq 15 from the DLS data for D and the SLS data for the osmotic compressibility by substituting the $M_w(c)$ obtained in the previous section in place of M. The values of $R_{H,app}$ thus determined at various T examined are listed along with the values of M_w in Tables 1 and 2 for the $C_{10}E_5$ and $C_{10}E_6$ micelles, respectively. They are double-logarithmically plotted against M_w in Figure 11 for the $C_{10}E_5$ micelles and in Figure 12 for the $C_{10}E_6$ micelles. As $M_w(c)$ is decreased with decreasing c, $R_{H,app}$ at each given T decreases, following a curve convex downward. The data points at different T seem to form asymptotically a single composite curve at small M_w, that is, at low c. These results imply that effects of intermicellar hydrodynamic interactions on $R_{H,app}$ become less significant as c is lowered and are negligible in the asymptotic region of low c. Thus, the data points at small $M_w(c)$ (low c) at each fixed

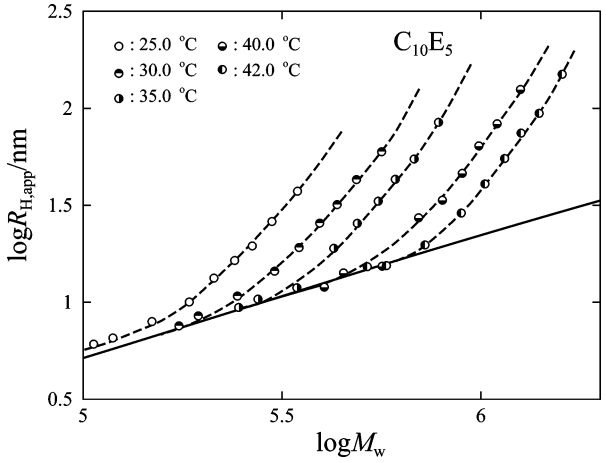

Figure 11. Double-logarithmic plots of $R_{H,app}$ against M_w for all the $C_{10}E_5$ solutions: The circles have the same meaning as those in Figure 4. The dashed curves are drawn to guide the eye. The solid curve represents the theoretical values calculated by eqs 16 and 17.

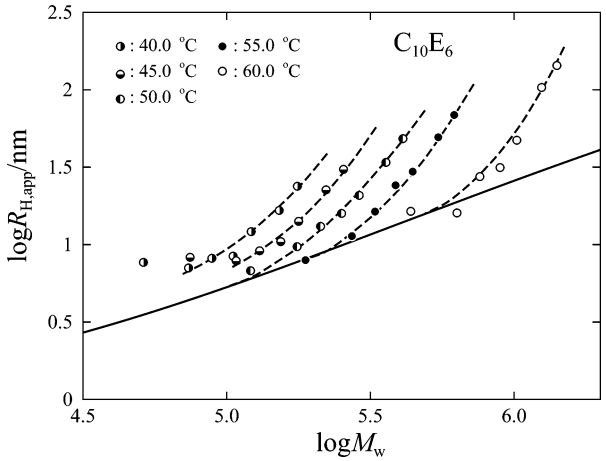

Figure 12. Double-logarithmic plots of $R_{H,app}$ against M_w for all the $C_{10}E_6$ solutions: The circles have the same meaning as those in Figure 5. The dashed curves are drawn to guide the eye. The solid curve represents the theoretical values calculated by eqs 16 and 17.

T may be regarded to give the relationship between R_H and M_w for the isolated micelles. These results are similar to the previous findings for $C_{12}E_6$ and $C_{14}E_6$ micelles[1] and for $C_{14}E_8$, $C_{16}E_8$, and $C_{18}E_8$ micelles.[2] On the other hand, $R_{H,app}(c)$ at any given T increases with increasing M_w or c, following a curve concave upward, reflecting two contributions: micellar growth in size and enhancement of the effects of the intermicellar hydrodynamic interactions with increasing c.

In this work, we analyze the data for the hydrodynamic radius R_H of the isolated $C_{10}E_5$ and $C_{10}E_6$ micelles by using the hydrodynamic theories formulated for the wormlike spherocylinder model. The translational diffusion coefficient D is formulated by Norisuye et al.[6] for the wormlike spherocylinder model and by Yamakawa et al.[7,8] for the wormlike cylinder model, as a function of L with including the parameters d and λ^{-1}. From these theories, we may derive the expression for R_H as a function of L, d, and λ^{-1} over the entire range of L, including the sphere, i.e., the case $L = d$. It reads

$$R_H = \frac{L}{2f(\lambda L, \lambda d)} \tag{16}$$

The expression for the function f is so lengthy that we refer it

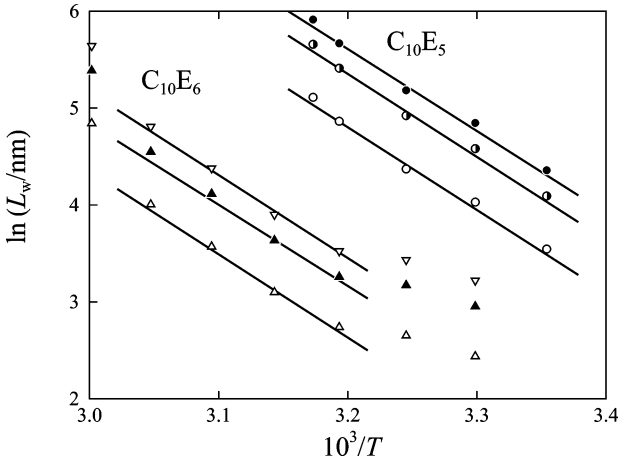

Figure 13. Plots of ln L against $1/T$ for the $C_{10}E_5$ (circles) and $C_{10}E_6$ micelles (triangles) at three concentrations: unfilled circles and triangles, 0.01 g/cm^3; half-filled circles and filled triangles, 0.03 g/cm^3; filled circles and top-down triangles, 0.05 g/cm^3.

to the original papers.[6−8] In the present analysis, we have calculated L_w using the relation

$$L_w = \frac{4vM_w}{\pi N_A d^2} + \frac{d}{3} \tag{17}$$

The L_w values obtained by this equation were used in place of L in eq 16.

The theoretical values of R_H have been calculated as a function of M_w for various values of λ^{-1}, with $d = 2.6$ nm for both $C_{10}E_5$ and $C_{10}E_6$ micelles, as discussed above. The solid lines in Figures 11 and 12 are the best-fit curves to the data points for the isolated micelles. It is found that the theoretical curves well describe the observed behavior of R_H as a function of M_w, except for the data at the lowest two temperatures 40.0 and 45.0 °C in Figure 12. The curve fitting yields λ^{-1} equal to 35.0 and 75.0 nm for the $C_{10}E_5$ and $C_{10}E_6$ micelles, respectively. These values are considerably larger than the previous results with λ^{-1} equal to 14.0 and 7.0 nm for $C_{12}E_6$ and $C_{14}E_6$ micelles, respectively.[1] The differences indicate that λ^{-1} is highly dependent on the hydrophobic chain length or the ratio of i to j of the surfactant C_iE_j molecule.

Micellar Length and Structure. The values of L_w calculated from M_w and d by eq 17 for the $C_{10}E_5$ and $C_{10}E_6$ micelles at observed T and c are summarized in Tables 1 and 2, respectively, along with those of M_w, D, and $R_{H,app}$. In Figure 13, L_w calculated for both micelles at three concentrations $c = 0.01$, 0.03, and 0.05 g/cm^3 are plotted in the form of lnL_w against $1/T$. The data set at given c roughly follows a straight line with the same slope irrespective of c, although strictly speaking, it follows a curve convex downward especially in the case of the $C_{10}E_6$ micelles. The results are in accord with eq 10 or eq 11. From the slope, we obtain energy of ca. −70 kJ/mol, which may correspond to Δg in eq 11, but not to the scission energy E_{sc} in eq 10, which should be positive. With positive E_{sc} in eq 10, $\langle L \rangle$ is expected to decrease with increasing T, contrary to the behavior observed here, for which L_w increases as T is raised or c is increased. When compared at the same c and T, the L_w value of the $C_{10}E_5$ micelle is considerably larger than that of the $C_{10}E_6$ micelle, indicating that the ratio of i to j of the surfactant C_iE_j molecule controls micellar length. However, $C_{10}E_5$ and $C_{10}E_6$ micelles grow in length to almost the same extent when the temperature approaches the lower consolute phase boundary for each micellar solution (see Figure 1). These results are in good correspondence with those for g_2 shown in Figure 10: the g_2 value for the $C_{10}E_5$ micelle solution is larger than that of the $C_{10}E_6$ micelle solution when compared at fixed T, but g_2 of both micelle solutions have almost the same value when T is close to the phase separation temperature.

To visualize the micellar structure, the spacing s between hydrophobic tails of adjacent surfactant molecules on the micellar surface has been evaluated from the values of d, L_w, and N_w calculated from M_w. The s value obtained is ca. 1.1 nm for $C_{10}E_5$ micelles and ca. 1.2 nm for $C_{10}E_6$ micelle, irrespective of c and T. According to the rotational isomeric state (RIS) model calculations by Flory,[22] the root mean-square end-to-end distance $\langle R^2 \rangle^{1/2}$ of pentaoxyethylene is 1.00 nm and that of hexaoxyethylene is 1.12 nm. The values of s are comparable to these values for both micelles. This approximate coincidence suggests that the hydrophilic tails of the surfactant molecules are moving by taking a random orientation in water. An RIS calculation for the n-decyl chain yields 0.87 nm as $\langle R^2 \rangle^{1/2}$. Thus, if it is assumed that the n-decyl chains of different surfactant molecules completely overlap in the hydrophobic core, as in the case of amorphous bulk polyethylene, and the hexaoxyethylene groups are oriented straightforwardly in the radial direction, the RIS calculations give d equal to 2.87 and 3.11 nm for $C_{10}E_5$ and $C_{10}E_6$ micelles, respectively. The value $d =$ 2.6 nm reported above is somewhat smaller than these values. The difference again suggests that the hydrophilic groups of C_iE_j molecules are rotating randomly on the micellar surface.

Conclusion

In this work, we have characterized $C_{10}E_5$ and $C_{10}E_6$ micelles in dilute solutions at several temperatures T below the lower consolute phase boundary by SLS and DLS measurements. The results of $Kc/\Delta R_0$ from SLS have been analyzed with the aid of the thermodynamic theory[3] for light scattering of micelle solutions formulated with the wormlike spherocylinder model. The analyses have yielded the molar mass $M_w(c)$ as a function of the surfactant mass concentration c and the cross-sectional diameter d of 2.6 nm for both $C_{10}E_5$ the $C_{10}E_6$ micelles. The good agreements between the calculated and observed $Kc/\Delta R_0$ as a function of c indicate that both micelles assume the shape of a flexible spherocylinder in dilute solutions. The micelles have been found to grow in size with increasing c or increasing T, following the relation $M_w(c) \propto c^{1/2}$, in line with the theoretical prediction[3,5] for highly extended polymer-like micelles.

The hydrodynamic radius R_H of the individual isolated $C_{10}E_5$ and $C_{10}E_6$ micelles as a function of M_w has been successfully described by the corresponding theories for the wormlike spherocylinder model. The values of the stiffness parameter λ^{-1} evaluated from the fitting theoretical values for R_H to the experimental results give larger λ^{-1} for $C_{10}E_5$ and $C_{10}E_6$ micelles than that for C_iE_j micelles studied previously,[1,2] with λ^{-1} about twice as large for $C_{10}E_6$ micelles than the value for $C_{10}E_5$ micelles.

Both $C_{10}E_5$ and $C_{10}E_6$ micelles grow in length to an almost equal extent in the region of c and T close to the phase boundary of each micelle solution. In conformity with the results, the free energy parameter g_2 is approximately the same for the two micelle solutions at corresponding c and T. However, when compared at fixed c and T, $C_{10}E_5$ micelles are much longer than $C_{10}E_6$ micelles, and correspondingly the g_2 value is larger in the former micelle solutions than in the latter. The cross-sectional diameter d of cylindrical micelles and the spacing s of adjacent hydrophilic chains on the micellar surface have been found to be almost the same for both $C_{10}E_5$ and $C_{10}E_6$ micelles.

Acknowledgment. The authors are grateful to members of the NKO Academy for valuable discussions and comments. This research was supported in part by Nara Women's University Intramural Grant for Project Research.

Appendix: Light Scattering Theory for Micelle Solutions

In what follows, the equations required to calculate $Kc/\Delta R_0$ by eq 12 are briefly summarized. On the basis of the multiple equilibrium conditions among micelles, Sato[3] has derived the expression of M_w as:

$$M_w = M_0 N_w = M_0\left[\frac{(1+\xi)^2 + X}{(1-X)(1+\xi)}\right] \tag{18}$$

with M_0 being the molecular weight of the surfactant molecule and N_w the weight-average aggregation number of the micelle. The quantities X and ξ are defined as:

$$\ln X \equiv (1/N_e)[F_2(N_n,\phi) + g_2 + \ln\phi_e - \ln(N_e/\rho')] \tag{19}$$

$$\xi \equiv (N_e - 1)(1 - X) \tag{20}$$

Here, g_2 is the free energy parameter and N_e is the number of surfactant molecules contained in the two hemispheres at the ends of the spherocylinder given as

$$N_e = (\pi/6)d^3\rho' \tag{21}$$

where d is the cross-sectional diameter of the spherocylinder and ρ' is the number density of the surfactant molecule in the micelle given by

$$\rho' = N_A/\upsilon M_0 \tag{22}$$

with υ being the partial specific volume of the micelle. The number-average aggregation number N_n is derived as

$$N_n = (1+\xi)/(1-X) \tag{23}$$

In eq 19, ϕ and ϕ_e are the volume fraction of the total micelles in the solution and the equilibrium volume fraction of the smallest micelles, respectively. The former is related to the latter by

$$\phi = \frac{(1+\xi)\phi_e}{(1-X)^2 N_e} \tag{24}$$

and also to c by $\phi = \upsilon c$. Function $F_2(N_n,\phi)$ is given by

$$F_2(N_n,\phi) = \frac{5}{3}\frac{\phi}{(1-\phi)}\left\{1 + \frac{4N_e}{5N_n} + \frac{2}{5}\left[1 + \frac{N_e}{N_n} + \frac{1}{4}\left(\frac{N_e}{N_n}\right)^2\right]\frac{\phi}{(1-\phi)}\right\} - \ln(1-\phi) + \frac{2}{\pi}\left(2 + \frac{N_e}{N_n}\right)\Psi(\hat{\epsilon})\phi \tag{25}$$

with

$$\Psi(\hat{\epsilon}) = \frac{P^{(1)}[f^{(1)}]^2\hat{\epsilon}}{f^{(1)} - {}^1/_2 f^{(2)}\hat{\epsilon}} \tag{26}$$

and

$$f^{(i)} \equiv 1 - \frac{\alpha^{(i)}C^{(i)}}{\beta^{(i)}} + \frac{6}{\pi}Q^{(i)}\phi + \frac{\pi C^{(i)}}{6\phi}\left\{1 - \exp\left[-\frac{\alpha^{(i)}\phi}{{}^1/_6\pi\beta^{(i)} - \phi}\right]\right\} \tag{27}$$

Here, the values of $P^{(i)}$, $Q^{(i)}$, $C^{(i)}$, $\alpha^{(i)}$, and $\beta^{(i)}$ are given in the following:[17]

i	$P^{(i)}$	$Q^{(i)}$	$C^{(i)}$	$\alpha^{(i)}$	$\beta^{(i)}$
1	−4.97419	0.487962	1.700943	1.5	$2^{1/2}$
2		−3.98844	−3.19927	2.75	$2^{1/2}$

The parameter $\hat{\epsilon}$ represents the strength of the intermicellar attractive interaction. The apparent virial coefficient A is represented as

$$A = \frac{\pi d^3 N_A}{9M_0^2 N_e^2}\left[\frac{1+\phi}{(1-\phi)^4} + \frac{3}{2\pi}\Psi(\hat{\epsilon}) + \frac{3}{\pi}\frac{d\Psi(\hat{\epsilon})}{d\phi}\phi + \frac{3}{4\pi}\frac{d^2\Psi(\hat{\epsilon})}{d\phi^2}\phi^2\right] \tag{28}$$

With known values of M_0 and υ, we can obtain the X value at given ϕ (or c) by solving eq 19 with the use of eqs 20−27, for a set of values of the parameters d, g_2, and $\hat{\epsilon}$. The X value thus determined allows us to calculate $M_w(c)$ by substituting it into eq 18 along with the values of M_0 and ξ calculated by eq 20. By using the values of $M_w(c)$ along with those of $A(c)$ calculated by eq 28 as a function of ϕ (or c) for the same set of the values of d and $\hat{\epsilon}$, $Kc/\Delta R_0$ is calculated as a function of c by eq 12.

References and Notes

(1) Yoshimura, S.; Shirai, S.; Einaga, Y. *J. Phys. Chem. B* **2004**, *108*, 15477.
(2) Hamada, N.; Einaga, Y. *J. Phys. Chem. B.* Submitted for publication.
(3) Sato, T. *Langmuir* **2004**, *20*, 1095.
(4) Cates, M. E.; Candou, S. J. *J. Phys. Condens. Matter* **1990**, *2*, 6869 and references therein.
(5) Zoeller, N.; Lue. L.; Blankschtein, D. *Langmuir* **1997**, *13*, 5258.
(6) Norisuye, T.; Motowoka, M.; Fujita, H. *Macromolecules* **1979**, *12*, 320.
(7) Yamakawa, H.; Fujii, M. *Macromolecules* **1973**, *6*, 407.
(8) Yamakawa, H.; Yoshizaki, T. *Macromolecules* **1979**, *12*, 32.
(9) Benoit, H.; Doty, P. *J. Phys. Chem.* **1953**, *57*, 958.
(10) Huibers, P. D. T.; Shah, D. O.; Katritzky, A. R. *J. Colloid Interface Sci.* **1997**, *193*, 132.
(11) Pike, E. R.; Pomeroy, R. M.; Vaughan, J. M. *J. Chem. Phys.* **1975**, *62*, 3188.
(12) Einaga, Y.; Mitani, T.; Hashizume, J.; Fujita, H. *Polym. J.* **1979**, *11*, 565.
(13) Lang, J. C.; Morgan, R. D. *J. Chem. Phys.* **1980**, *73*, 5849.
(14) Magid, L. J. *J. Phys. Chem. B* **1998**, *102*, 4064.
(15) Blankschtein. D.; Thurston, G. M.; Benedek, G. B. *J. Chem. Phys.* **1986**, *85*, 7268.
(16) Puvvada, S.; Blankschtein, D. *J. Chem. Phys.* **1990**, *92*, 3710.
(17) Koyama, R.; Sato, T. *Macromolecules* **2002**, *35*, 2235.
(18) Casassa, E. F.; Berry, G. C. Polymer Solutions. In *Comprehensive Polymer Science*; Allen, G., Ed.; Pergamon Press: New York, 1988.
(19) Berry, G. C. *Adv. Polym. Sci.* **1994**, *114*, 233.
(20) Berne, B.; Pecora, R. *Dynamic Light Scattering*; J. Wiley: New York, 1976.
(21) Stepánek, P.; Brown, W.; Hvidt, S. *Macromolecules* **1996**, *29*, 8888.
(22) Flory, P. J. *Statistical Mechanics of Chain Molecules*; John Wiley & Sons: New York, 1969.